

The planetary nebula nature and properties of IRAS 18197–1118^{*†}

L. F. Miranda^{1,2‡§}, L. F. Rodríguez^{3‡}, C. B. Pereira^{4‡}, R. Vázquez^{5‡}

¹ Consejo Superior de Investigaciones Científicas, C/ Serrano 117, E-28006 Madrid, Spain

² Departamento de Física Aplicada, Facultad de Ciencias, Campus Lagoas-Marcosende s/n, Universidade de Vigo, E-36310 Vigo, Spain (present address)

³ Centro de Radioastronomía y Astrofísica, Universidad Nacional Autónoma de México, Apartado Postal 3-72, Morelia, Michoacán 58089, Mexico

⁴ Observatório Nacional, Rua José Cristino, 77. CEP 20921-400, São Cristóvão, Rio de Janeiro-RJ, Brazil

⁵ Instituto de Astronomía, Universidad Nacional Autónoma de México, Apdo. Postal 877, 22800 Ensenada, BC, Mexico

Accepted . Received ; in original form

ABSTRACT

IRAS 18197–1118 is a stellar-like object that has been classified as a planetary nebula from its radio continuum emission and high [S III] λ 9532 to Paschen9 line intensity ratio, as derived from direct images. We present intermediate- and high-resolution, optical spectroscopy, VLA 8.46 GHz radio continuum data, and narrow-band optical images of IRAS 18197–1118 aimed at confirming its planetary nebula nature, and analyzing its properties. The optical spectrum shows that IRAS 18197–1118 is a medium-excitation planetary nebula suffering a high extinction ($A_{H\beta} \simeq 3.37$). The optical images do not resolve the object but the 8.46 GHz image reveals an elliptical shell of $\simeq 2.7 \times 1.6$ arcsec² in size, a compact central nebular region, and possible bipolar jet-like features, indicating several ejection events. The existence of a compact central nebula makes IRAS 18197–1118 singular because this kind of structure is observed in a few PNe only. An expansion velocity $\simeq 20$ km s⁻¹ and a systemic velocity (LSR) $\simeq +95$ km s⁻¹ are obtained for the object. An electron density of $\simeq 3.4 \times 10^4$ cm⁻³ and an ionized mass of $\simeq 2.1 \times 10^{-2} M_{\odot}$ are deduced from the 8.46 GHz radio continuum data for an estimated statistical distance of 6 kpc. Helium abundance is high but nitrogen is not enriched, which is not consistently reproduced by evolutionary models, suggesting different abundances in the elliptical shell and central region. The properties of IRAS 18197–1118 indicate a relatively young planetary nebula, favor a distance of $\gtrsim 6$ kpc, and strongly suggest that it is an inner-disc planetary nebula.

Key words: planetary nebula: individual (IRAS 18197–1118) – interstellar medium: jets and outflows – interstellar medium: abundances

1 INTRODUCTION

Planetary nebulae (PNe) are the evolutionary phase of low- and intermediate-mass stars ($M \simeq 0.8\text{--}10 M_{\odot}$), between the asymptotic giant branch and the white dwarf phase. They

are key objects to study phenomena taking place during the late evolution of low- and intermediate-mass stars as, e.g., the mass ejection in the asymptotic giant branch, the formation of complex PNe, and the return of processed material to the interstellar medium, among others. In these studies, a precise knowledge of the total number of PNe and their properties is crucial. Remarkably, there exists a large discrepancy between the known and predicted number of PNe in the Galaxy, being the predicted number larger or much larger than the known one (see, e.g., Jacoby et al. 2010 and references therein). In recent years, surveys in different wavelength ranges have provided the opportunity of identifying large amounts of new PN candidates (e.g., Helfand et al. 1992; Condon, Kaplan & Terzian 1999; Parker et al. 2006; Miszalski et al. 2008; Viironen et al. 2009; Jacoby et al. 2010; Ramos-Larios et al. 2012), many of which have al-

* Based on observations collected at the German-Spanish Astronomical Center, Calar Alto, jointly operated by the Max-Planck-Institut für Astronomie (Heidelberg) and the Instituto de Astrofísica de Andalucía (CSIC).

† Based upon observations acquired at the Observatorio Astronómico Nacional in the Sierra San Pedro Mártir (OAN-SPM), Baja California, Mexico.

‡ E-mail: lfm@iaa.es (LFM); l.rodriguez@crya.unam.mx (LFR); claudio@on.br (CBP), vazquez@astrosen.unam.mx (RV)

§ LFM is Personal Desplazado of CSIC on temporal leave at the University of Vigo

ready been confirmed as true PNe by optical spectroscopy (e.g., Parker et al. 2006). As for the optical surveys, it is expected that only very few PNe have been missed in the surveyed areas, although compact (stellar-like), very low surface brightness, and/or highly extinguished PNe may be difficult to recognize (e.g., Miszalski et al. 2008). Identifying possible missing cases is interesting not only because they add to the number of known PNe but also because they may help refine automatic searches of PNe in large observational databases.

IRAS 18197–1118 [$\alpha(2000.0) = 18^{\text{h}} 22^{\text{m}} 30^{\text{s}}.0$, $\delta(2000.0) = -11^{\circ} 16' 44''$; $l = 019^{\circ} 6095$, $b = +01^{\circ} 1877$] is a stellar-like object that was identified as a PN candidate by Helfand et al. (1992) in an extension of the Galactic plane survey at 20 cm (Zoonematkermani et al. 1990). Subsequent radio continuum surveys have always detected the object. In particular, radio continuum emission from IRAS 18197–1118 has been detected also at 1.4 GHz with a flux density of 11.3 ± 0.7 mJy in the NRAO VLA Sky Survey (Condon et al. 1999), and at 4.86 GHz with a flux density of 60.7 ± 0.9 mJy in the VLA Red MSX Source (RMS) survey (Urquhart et al. 2009). Surprisingly, IRAS 18197–1118 has never been identified in any optical/infrared survey neither has it been included in analysis of PNe and PN candidates, with the exception of the work by Kistiakowsky & Helfand (1995, hereafter KH95). These authors did include IRAS 18197–1118 in their list of highly extinguished, presumably distant PN candidates to be confirmed through the $[\text{S III}]\lambda 9532/\text{Paschen } 9$ line intensity ratio as derived from direct images in these two lines. The high value of this ratio found in IRAS 18197–1118, as compared with that in H II regions, leads KH95 to propose a PN nature for the object. Even though this result and the presence of radio continuum emission favor that IRAS 18197–1118 is a PN, an analysis of its optical spectrum would be desirable to provide a firm confirmation of its nature, and to study its physical conditions and chemical abundances. In addition, the published VLA observations at 1.4 and 4.86 GHz (Condon et al. 1999; Urquhart et al. 2009) do not have spatial resolution enough to resolve IRAS 18197–1118 and, in consequence, its morphology is unknown.

We have carried out an analysis of intermediate- and high-resolution, optical spectra, VLA 8.46 GHz radio continuum data, and narrow-band optical images of IRAS 18197–1118 with the aim of confirming its PN nature and studying its properties. In this paper we present the results of this investigation.

2 OBSERVATIONS

2.1 Intermediate-resolution optical spectroscopy

Intermediate-resolution, long-slit spectra of IRAS 18197–1118 were obtained on Calar Alto Observatory (Almería, Spain) with the Calar Alto Faint Object Spectrograph (CAFOS) at the 2.2 m telescope on 2008 June 27. The detector was a SiTe CCD with 2048×2048 pixels. We used grisms B-100 and R-100 to cover the spectral ranges 3200–6200 Å and 5800–9600 Å, respectively, at a dispersion of $1.98 \text{ \AA pixel}^{-1}$. The slit (2 arcsec wide) was centered on the object and oriented at position angle (PA) 90° . The exposure time was 2400 s for each grism. The

spectrophotometric standard star BD+28°4211 was also observed for flux calibration. Sky was photometric during the observations and seeing was $\simeq 1$ arcsec. The spectra were reduced following standard procedures within the MIDAS and IRAF packages. We note that the flux calibration fails at the very red edge of the CCD, coinciding with the $[\text{S III}]\lambda 9532$ emission line detected in the spectrum. As a result, the flux of this emission line is unrealistic and it will not be considered further in this paper.

2.2 High-resolution optical spectroscopy

High-resolution, long-slit spectra were obtained with the Manchester Echelle Spectrometer (MES; Meaburn et al. 2003) at the 2.1 m telescope of the OAN-SPM¹ observatory during 2013 September 23. An e2v CCD with 2048×2048 pixels was used as detector, in the 2×2 binning mode ($0.6 \text{ arcsec pix}^{-1}$ plate scale). The slit length is 6.5 arcmin and its width was set to 2 arcsec. Spectra with the slit oriented at PA $+72^{\circ}$ and -18° were obtained using a $\Delta\lambda = 90 \text{ \AA}$ bandwidth filter to isolate the 87th order (0.1 \AA pix^{-1} dispersion), covering the H α and $[\text{N II}]\lambda\lambda 6548, 6583$ emission lines. In addition, a spectrum with the slit oriented at PA -18° was obtained using a $\Delta\lambda = 50 \text{ \AA}$ bandwidth filter to isolate the 114th order ($0.08 \text{ \AA pix}^{-1}$ dispersion), covering the $[\text{O III}]\lambda 5007$ emission line. Exposure time was 1800 seg for each spectrum. Seeing was $\simeq 1.8$ arcsec during the observations. Data were calibrated using standard techniques for long-slit spectroscopy in the IRAF package. The resulting spectral resolution (FWHM) is $\simeq 12 \text{ km s}^{-1}$ (accuracy $\pm 1 \text{ km s}^{-1}$), as measured from the lines of the ThAr calibration lamp.

2.3 Radio continuum observations

The radio observations of IRAS 18197–1118 were obtained from the archive of the Very Large Array (VLA) of the NRAO². These unpublished archive observations were made at 8.46 GHz in a snapshot of 8 minutes duration in 2005 January 19, under project AC761. The array was then in the BnA configuration. The data were edited and calibrated using the software package Astronomical Image Processing System (AIPS) of NRAO. The amplitude calibrator was 1331+305, with an adopted flux density of 5.21 Jy and the phase calibrator was 1832-105, with a bootstrapped flux density of 1.407 ± 0.003 Jy. The synthesized beam is $0.51 \times 0.28 \text{ arcsec}^2$ at PA 77° .

The integrated flux density of IRAS 18197–1118 at 8.46 GHz is 64.9 ± 0.6 mJy. A comparison of the fluxes at 1.4, 4.86, and 8.46 GHz indicates that the source is optically thin for frequencies above 8.46 GHz

¹ The Observatorio Astronómico Nacional at the Sierra de San Pedro Mártir, Baja California (OAN-SPM) is operated by the Instituto de Astronomía of the Universidad Nacional Autónoma de México (IA-UNAM).

² The National Radio Astronomy Observatory is operated by Associated Universities Inc. under cooperative agreement with the National Science Foundation.

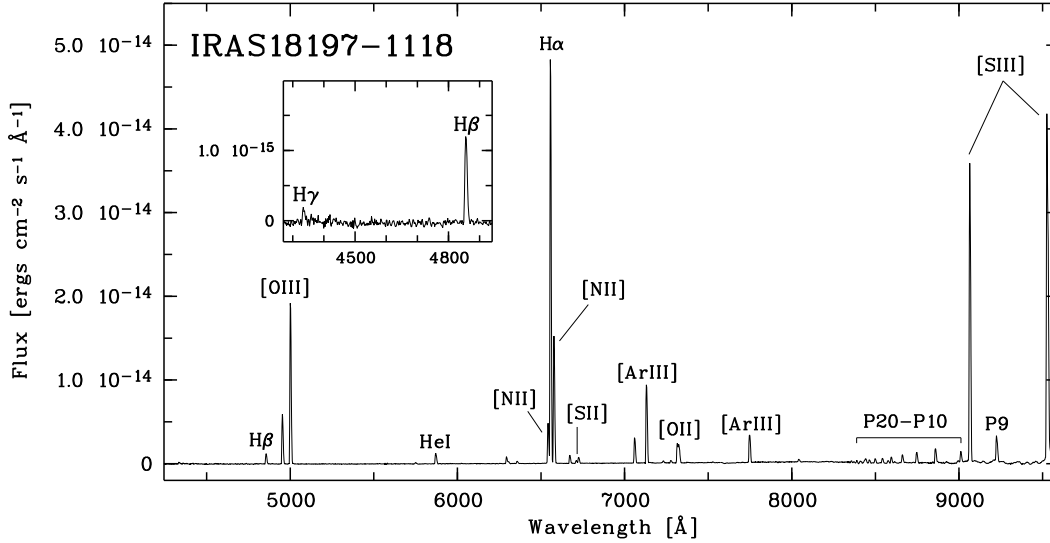


Figure 1. Blue and red CAFOS observed spectra of IRAS 18197–1118 in the spectral range 4245–9480 Å. Some emission lines are labelled. The inset shows the spectrum between the H γ and H β emission lines.

2.4 Optical images

Narrow-band optical images of IRAS 18197–1118 were obtained with the 1.5 m telescope of the Observatorio de Sierra Nevada (OSN)³ (Granada, Spain) on 2008 June 24. A RoperScientific VersArray with 2048×2048 pixels of 0.232×0.232 arcsec² each was used as detector. Images were obtained through three narrow-band filters in the light of H α (FWHM = 10 Å), [N II] λ 6583 (FWHM = 10 Å), and [O III] λ 5007 (FWHM = 50 Å). Exposure time was 1800 s for each filter. Seeing was \simeq 1.7 arcsec during the observations. The images were reduced following standard procedures within the MIDAS package.

3 RESULTS

3.1 The optical spectrum

Figure 1 presents the blue and red CAFOS spectra of IRAS 18197–1118. Hydrogen and neutral helium recombination emission lines and several forbidden emission lines in different excitation states can be recognized, as well as a faint nebular continuum. We note that the He II λ 4686 and [O III] λ 4363 emission lines are not detected in our spectrum. In particular, an upper limit of 3.4×10^{-16} erg cm⁻² s⁻¹ is obtained for the observed flux in the [O III] λ 4363 emission line. The observed H β flux is $\simeq 1.12 \times 10^{-14}$ erg cm⁻² s⁻¹.

We use the H α /H β and H β /H γ observed flux ratios to calculate the logarithmic extinction coefficient ($c_{H\beta}$) assuming case B recombination, theoretical H α /H β and H β /H γ line ratios of 2.85 and 2.13, respectively (Brocklehurst 1971), and the extinction curve by Seaton (1979). We obtain $c_{H\beta} \simeq 3.50$ from the H α /H β ratio and $\simeq 3.25$ from the H β /H γ ratio. Besides, the flux density at 8.46 GHz and the H β flux

Table 1. Dereddened line intensities in IRAS 18197–1118 in units of $I_{H\beta} = 100.0$

Line	$f(\lambda)$	$I(\lambda)$
He I λ 3889	0.223	58 ± 7
H γ λ 4340	0.129	48.5 ± 3.9
H β λ 4861	0.000	100.0 ± 1.5
[O III] λ 4959	-0.023	413.0 ± 5.6
[O III] λ 5007	-0.034	1231.7 ± 13.1
[N II] λ 5755	-0.191	4.0 ± 0.2
He I λ 5876	-0.216	22.1 ± 0.3
[O I] λ 6300	-0.285	5.6 ± 0.1
[S III] λ 6312	-0.287	3.3 ± 0.1
[O I] λ 6363	-0.294	2.6 ± 0.1
[N II] λ 6548	-0.321	28.9 ± 3.1
H α λ 6563	-0.323	315.2 ± 6.7
[N II] λ 6584	-0.326	101 ± 3
He I λ 6678	-0.338	5.8 ± 0.1
[S II] λ 6716	-0.343	1.8 ± 0.1
[S II] λ 6731	-0.345	4.3 ± 0.1
He I λ 7065	-0.383	13.7 ± 0.2
[Ar III] λ 7135	-0.391	40.7 ± 0.5
He I λ 7281	-0.406	1.2 ± 0.1
[O II] λ 7325	-0.411	16.3 ± 0.2
[Ar III] λ 7751	-0.451	9.7 ± 0.1
P 20 λ 8392	-0.509	0.16 ± 0.02
P 19 λ 8413	-0.512	0.21 ± 0.02
P 18 λ 8438	-0.516	0.91 ± 0.02
P 17 λ 8467	-0.521	0.39 ± 0.02
P 16 λ 8502	-0.526	0.72 ± 0.02
P 15 λ 8545	-0.532	0.84 ± 0.02
P 14 λ 8598	-0.540	0.98 ± 0.02
P 13 λ 8665	-0.550	1.17 ± 0.02
P 12 λ 8750	-0.562	1.46 ± 0.02
P 11 λ 8863	-0.578	1.79 ± 0.03
P 10 λ 9015	-0.599	1.06 ± 0.02
[S III] λ 9069	-0.606	29.1 ± 0.3
P 9 λ 9229	-0.612	2.79 ± 0.04
$\log F_{H\beta}$	-13.95	(erg cm ⁻² s ⁻¹)
$c_{H\beta}$	3.37	

³ The Observatorio de Sierra Nevada is operated by the Consejo Superior de Invetigaciones Cientificas through the Instituto de Astrofísica de Andalucía (Granada, Spain).

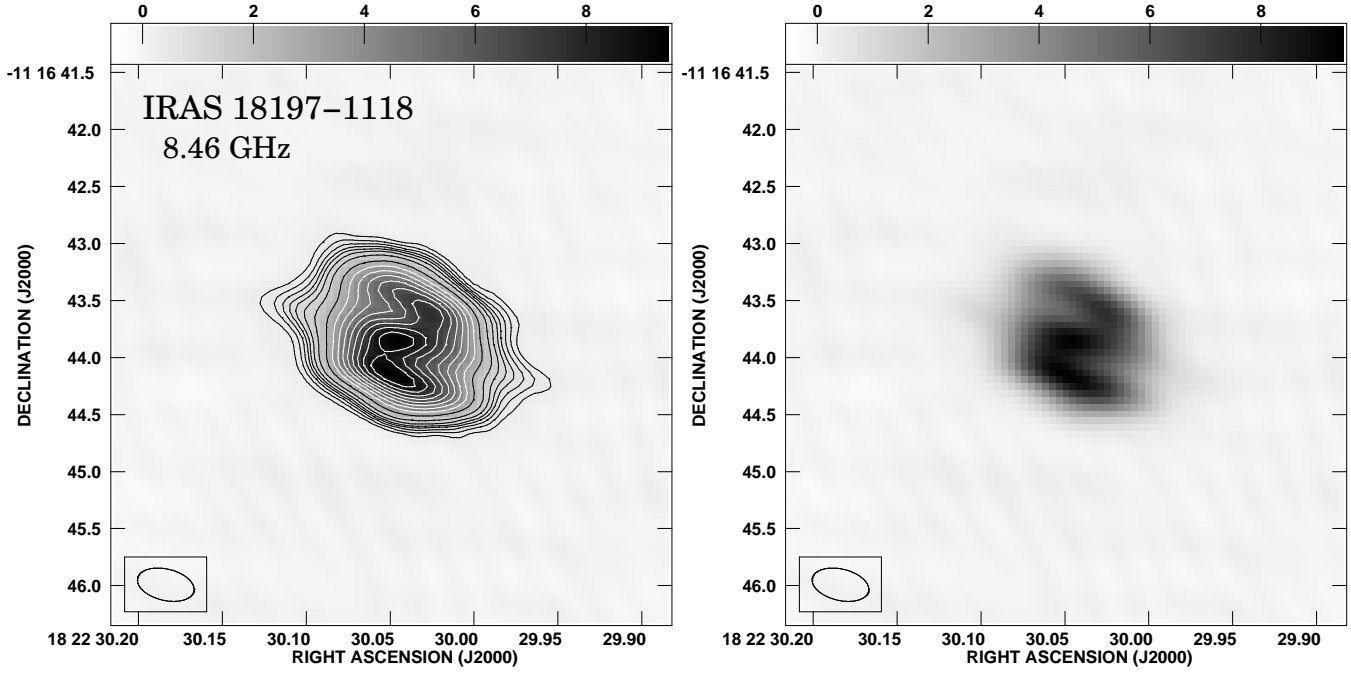


Figure 2. VLA image of IRAS 18197–1118 at 8.46 GHz in contours and grey scale (left panel), and grey scale (right panel). The contours are -4, 4, 6, 8, 10, 12, 15, 20, 30, 40, 50, 60, 70, 80, 90, 100, and 110 times $0.079 \text{ mJy beam}^{-1}$, the rms noise of the image. The greyscale values are given in the upper wedge in units of mJy beam^{-1} . The synthesized beam, with dimensions of $0.51 \times 0.28 \text{ arcsec}^2$ and major axis at position angle 77° , is shown in the bottom left corner of each panel.

can be used to derive $c_{\text{H}\beta} \simeq 3.55$ (see Pottasch 1984), similar to the values obtained from the Balmer decrement. In the following, we will adopt $c_{\text{H}\beta} = 3.37$ as the mean value from the Balmer lines and note that the main conclusions of this work do not depend on the assumed value of $c_{\text{H}\beta}$ in the 3.25–3.55 range.

Table 1 presents the dereddened emission line intensities obtained from the spectrum, as well as their Poissonian errors. The $[\text{N II}]\lambda\lambda 6548, 6583/\text{H}\alpha$ and $[\text{S II}]\lambda\lambda 6716, 6731/\text{H}\alpha$ line intensity ratios of $\simeq 0.41$ and $\simeq 0.02$, respectively, place IRAS 18197–1118 in the PN region of the $[\text{N II}]/\text{H}\alpha$ vs. $[\text{S II}]/\text{H}\alpha$ diagram (see, e.g., Frew & Parker 2010), confirming its PN nature. These two line intensity ratios, the $[\text{O III}]\lambda\lambda 4959, 5007/\text{H}\beta$ line intensity ratio of $\simeq 16$ (Table 1), and the absence of $\text{He II}\lambda 4686$ line emission indicate a medium-excitation PN.

3.2 Morphology

Figure 2 shows reproductions of the image of IRAS 18197–1118 at 8.46 GHz in which the nebula is resolved. The brightest nebular regions present a Z-shaped morphology (Fig. 2, right) formed by two arcs and a bright, compact central region. When lower intensity levels are considered (Fig. 2, left), the arcs trace the brightest parts of an elliptical shell with a size of $\simeq 2.7 \times 1.6 \text{ arcsec}^2$ and the major axis oriented at $\text{PA} \simeq 73^\circ$. The twisted appearance of the arcs delineates a point-symmetry in the elliptical shell, that is similar to that observed in other point-symmetric elliptical PNe (e.g., Miranda et al. 1997; Guerrero et al. 2001). Two faint, elongated bipolar protrusions, separated by $\simeq 2.2 \text{ arcsec}$, are observed along the major nebular

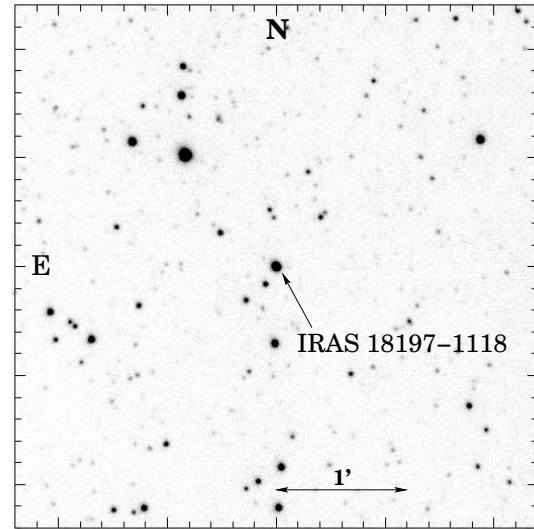


Figure 3. Identification chart of IRAS 18197–1118 (arrowed) derived from the OSN $[\text{N II}]$ image.

axis of the elliptical shell. Their morphology suggests that they could be jet-like features. However, as the protrusions are elongated in a similar direction to that of the beam (Fig. 2), the reality of these features needs confirmation. The bright central region seems to be elongated close to the east-west direction, although it is not resolved by the observations (size $\lesssim 0.5 \text{ arcsec}$) and analyzing its morphology requires higher spatial resolution. We note that the detection of the central region at radio continuum wavelengths implies a nebular structure and not emission

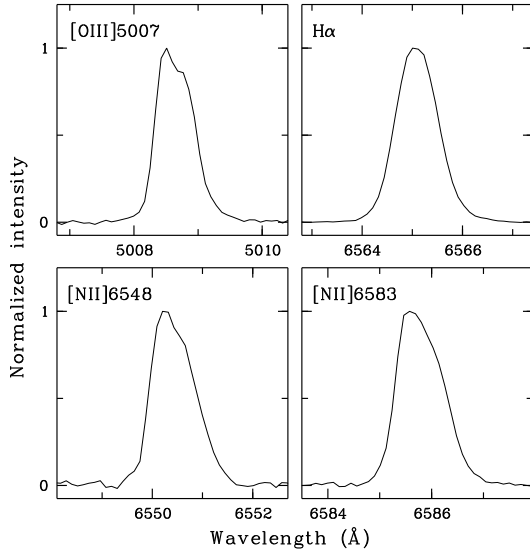


Figure 4. Normalized emission line profiles derived from the high-resolution, long-slit spectra.

from the central star. The existence of this region clearly shows that IRAS 18197–1118 does not exhibit a hollow shell as expected in PNe, indicating that a complex mass loss history, possibly related to several ejection events, has been implied in the formation of this object.

Figure 3 shows an identification chart for IRAS 18197–1118 based on the OSN [N II] image. The object appears relatively bright in the three filters ($H\alpha$ and [O III] images not shown here), although no internal structure can be recognized at the (relatively low) spatial resolution of our images, but only a stellar-like object.

3.3 Kinematics

The high-resolution, long-slit spectra do not resolve details of the spatial structure of IRAS 18197–1118, given the inadequate spatial resolution for such a small object. Thus, the spectra do not allow us to clarify whether the bipolar protrusions (Fig. 2) are real, because faint emission from these features could be superposed by the stronger one from the elliptical shell.

Figure 4 shows the integrated spectral profiles of the four observed emission lines. The $H\alpha$ emission line presents a single peaked, symmetric profile, while the [N II] and [O III] emission line profiles are asymmetric, suggesting that they are composed by at least two partially resolved velocity components. By using a two component Gaussian line fit, we obtain a radial velocity separation between the two velocity components of $\simeq 26 \text{ km s}^{-1}$ in [N II] and $\simeq 22 \text{ km s}^{-1}$ in [O III], which would imply a nebular expansion velocity of $\simeq 13$ and $\simeq 11 \text{ km s}^{-1}$ in [N II] and [O III], respectively. However, because the emission lines are not well resolved, these values probably correspond to lower limits to the expansion velocity. We can consider the FWHM of the emission lines as more representative of the expansion velocity. In this case, and correcting of spectral resolution (§ 2.2), we obtain an expansion velocity of $\simeq 22$ and $\simeq 19 \text{ km s}^{-1}$ in [N II] and [O III], respectively. These values should also be seen with caution because the FWHM does not discriminate velocity compo-

Table 2. Ionic abundances relative to H^+ in IRAS 18197–1118.

Ion ^a	Ionic abundance
He^+	0.145 ± 0.002
O^0	$8.5 \pm 1.7 \times 10^{-6}$
O^+	$4.1 \pm 1.2 \times 10^{-5}$
O^{2+}	$3.1 \pm 0.5 \times 10^{-4}$
N^+	$2.0 \pm 0.4 \times 10^{-5}$
S^+	$7.2 \pm 1.1 \times 10^{-6}$
S^{2+}	$5.8 \pm 0.7 \times 10^{-6}$
Ar^{2+}	$2.9 \pm 0.3 \times 10^{-6}$

^a For ions with more than one transition, an intensity-weighted average has been used.

Table 3. Elemental abundances in IRAS 18197–1118.

Element ratio	Abundance
He/H	0.145 ± 0.002
O/H	$3.5 \pm 0.5 \times 10^{-4}$
N/H	$1.7 \pm 0.6 \times 10^{-4}$
S/H	$9.7 \pm 3.7 \times 10^{-6}$
Ar/H	$5.4 \pm 0.3 \times 10^{-6}$
N/O	0.48 ± 0.17

nents that have not been spatially resolved and/or move almost perpendicular to the line of sight. In any case, with an expansion velocity of 20 km s^{-1} and the deconvolved size (0.85 arcsec , see above), a crude estimate for the kinematical age of $\simeq 100 \times D[\text{kpc}] \text{ yr}$ is obtained, which, at a distance D of 6 kpc (see § 3.4), results to be $\simeq 600 \text{ yr}$, pointing out to a relatively young PN. Finally, from the centroid of the emission line profiles we obtain a systemic velocity $V_{\text{LSR}} = +95 \pm 1.5 \text{ km s}^{-1}$ ($V_{\odot} = +80 \pm 1.5 \text{ km s}^{-1}$) for IRAS 18197–1118.

3.4 Physical conditions and chemical abundances

The [S II] $\lambda 6716/\lambda 6730$ line intensity ratio of $\simeq 0.42$ (Table 1) is at the lower sensitivity limit for electron density (N_e) measurement, indicating $N_e > 2 \times 10^4 \text{ cm}^{-3}$. The electron density and ionized mass (M_i) can be obtained from the radio continuum emission following the formulation by Mezger & Henderson (1967) for optically thin emission (see also Gómez, Rodríguez & Loinard 2013). With the flux at 8.46 GHz , the deconvolved radius at 8.46 GHz , and an electron temperature $T_e = 10000 \text{ K}$, we obtain $N_e \simeq 8.23 \times 10^4 \times D[\text{kpc}]^{-0.5} \text{ cm}^{-3}$ and $M_i \simeq 2.4 \times 10^{-2} \times D[\text{kpc}]^{2.5} M_{\odot}$. The distance to the nebula is involved in the calculations of these two parameters but is unknown for IRAS 18197–1118. We use the statistical distance scale by Zhang (1995) to obtain a value of $\simeq 6 \text{ kpc}$ that will be used through the paper (see also § 4). With this distance, the electron density and ionized mass are $3.36 \pm 0.50 \times 10^4 \text{ cm}^{-3}$ and $2.1 \pm 0.3 \times 10^{-2} M_{\odot}$, respectively. The electron density is relatively high and compatible with the lower limit indicated by the [S II] emission lines. The ionized mass is relatively small. The values of these two parameters suggest that IRAS 18197–1118 is a young PN.

The detection of the auroral and nebular [N II] emission lines (Table 1) allows us to obtain the electron temperature

$T_e([\text{N II}])$. We have used the task `temden` in IRAF and the value obtained for N_e to derive $T_e([\text{N II}]) = 11160 \pm 575$ K. We note that, because of the weak dependence of N_e and M_i on T_e (N_e and $M_i \propto [T_e/10^4]^{0.175}$, see, e.g., Gómez et al. 2013), the use of $T_e = 10000$ K or 11160 K to calculate N_e and M_i is not critical.

Ionic and elemental abundances have been obtained for the values of N_e and $T_e([\text{N II}])$ quoted above. For the ionic abundances we used the task `ionic` of IRAF and they are listed in Table 2. Total elemental abundances have been calculated using the `icf` method by Kingsburgh & Barlow (1994). For the helium abundance, we follow the formulation by Clegg (1987). The elemental abundances are listed in Table 3. In Figure 5 we show a $12 + \log(\text{S}/\text{H})$ vs. $12 + \log(\text{O}/\text{H})$ abundance diagram to analyze the Peimbert type (Peimbert 1990) of IRAS 18197–1118.

The position of IRAS 18197–1118 in Fig. 5 rules out a type IV (halo) PN while type I and type II PNe cannot be distinguished in this diagram. The high helium abundance ($\text{He}/\text{H} \simeq 0.14$) indicates a type I PNe. The N/O abundance ratio of ~ 0.48 (Table 3) seems compatible with a type I PN ($\text{N}/\text{O} \geq 0.5$, Peimbert 1978), although the involved errors do not allow us to draw a definitive conclusion. We note that a N/O abundance ratio of 0.65–0.8 has been considered by Kingsburgh & Barlow (1994) and Henry, Kwitter & Balick (2004) as a lower limit for type I PNe. With this criterion, the N/O abundance ratio classifies IRAS 18197–1118 as a type II PN. This classification is compatible with the nitrogen abundance (Table 3) that is much lower than that observed in type I PNe. Chemical abundances in PNe are related to the evolution of the progenitor star and, in particular, to its mass. In this respect, the double classification of IRAS 18197–1118 presents some contradictions. While a type II classification suggests a relatively low-mass progenitor, a type I one requires a relatively massive progenitor (e.g., Corradi & Schwarz 1995). It is interesting to mention that other type II PNe also show a high helium abundance typical of type I PNe (see Henry et al. 2004).

To obtain more precise information about the properties of the IRAS 18197–1118 progenitor, we have compared the obtained abundances (Table 3) with those predicted from the evolutionary models by Marigo (2001) and Karakas (2010). According to Marigo’s (2001) models, the obtained N and O abundances suggest a $1.3\text{--}1.5 M_\odot$ progenitor, although with a different metallicity, $Z = 0.019$ for N, and $Z = 0.008$ for O. However, the observed He abundance requires a progenitor mass $> 4 M_\odot$ for any metallicity. Using the Karakas’ (2010) models, the obtained N abundance points out to a $2.5 M_\odot$ progenitor with $Z = 0.02$, while the obtained O abundance is not well reproduced, and only models with $2 M_\odot$ produce approximated values. As for the He abundance, Karakas’ models predict (much) lower values than the obtained one, even considering a $6 M_\odot$ progenitor. We note the existence of noticeable discrepancies between the predictions of the two models, which could be attributable to the many different assumptions included in each model. However, both models coincide in that the observed He abundance requires a much more massive progenitor than indicated by the observed N and O abundances. In the case of IRAS 18197–1118 this could be related to the presence of two different nebular regions, the elliptical shell

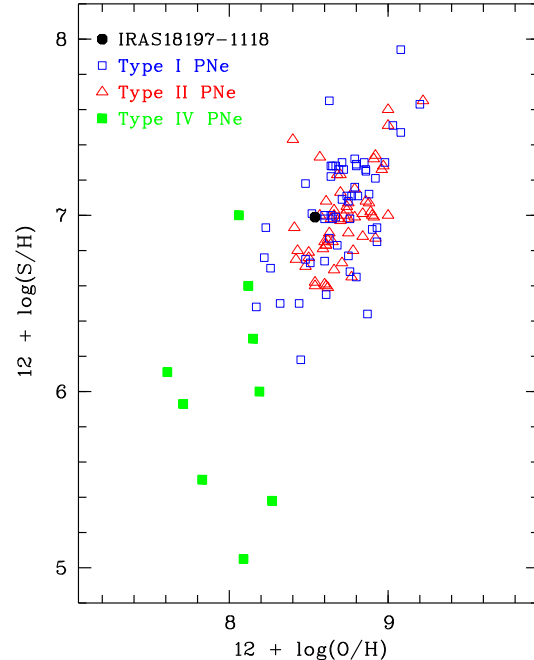


Figure 5. Plot of $12 + \log(\text{S}/\text{H})$ vs. $\log(\text{O}/\text{H})$ for the four Peimbert types of PNe. The data are taken from Maciel & Köppen (1994), Howard, Henry & McCartney (1997), and Pereira & Miranda (2007). The position of IRAS 18197–1118 is indicated (see Table 3) (see the electronic version for a colour version of this figure).

and the central region, each with different abundances (see § 4).

4 DISCUSSION

Our data have confirmed that IRAS 18197–1118 is a true PN and have allowed us to deduce many of its properties. The values obtained for the electron density, ionized mass, and kinematical age indicate a relatively young PN. Particularly interesting is the high extinction towards the object. The value of $c_{\text{H}\beta} \simeq 3.25\text{--}3.55$ found in IRAS 18197–1118 is high for PNe and higher than the $c_{\text{H}\beta}$ values found in the large sample of PNe analyzed by Stasińska et al. (1992).

IRAS 18197–1118 is also atypical in that it contains a compact central nebular region inside an extended elliptical shell. There are only a few PNe that show a compact central nebula besides an extended (and typical) elliptical or bipolar shell, as, e.g., M 2-29, EGB 6, M 2-48 (Gesiki et al. 2010 and references therein), IC 4997 (Miranda & Torrelles 1998), and KjPn 8 (Vázquez, Kingsburgh & López 1998). The existence of the central nebular region and the elliptical shell indicates that the formation of IRAS 18197–1118 has been complex, involving at least two different mass ejection events. Moreover, it is reasonable to assume that the two ejections are not coeval but the formation of the elliptical shell has preceded that of the central region. If so, the chemical abundances (and physical conditions) in the central region could be different from those in the elliptical shell. Because the object is not spatially resolved in the spectra, the contribution of each structure to the (integrated) emission line intensities cannot be determined, and the deduced abundances (and physical

Table 4. Electron density, electron temperature, ionized mass, and elemental abundances in IRAS 18197–1118 for distances of 2 and 10 kpc.

Parameter	$D = 2$ kpc	$D = 10$ kpc
N_e (cm^{-3})	$5.82 \pm 0.87 \times 10^4$	$2.60 \pm 0.39 \times 10^4$
$T_e(\text{[N II]})$ (K)	9350 ± 415	12000 ± 700
M_i (M_\odot)	$1.3 \pm 0.2 \times 10^{-3}$	$7.5 \pm 0.9 \times 10^{-2}$
He/H	0.144 ± 0.003	0.146 ± 0.002
O/H	$7.0 \pm 1.0 \times 10^{-4}$	$2.8 \pm 0.5 \times 10^{-4}$
N/H	$2.5 \pm 0.9 \times 10^{-4}$	$1.3 \pm 0.5 \times 10^{-4}$
S/H	$1.4 \pm 0.5 \times 10^{-5}$	$8.1 \pm 3.8 \times 10^{-6}$
Ar/H	$8.2 \pm 0.4 \times 10^{-6}$	$4.7 \pm 0.3 \times 10^{-6}$
N/O	0.35 ± 0.12	0.46 ± 0.19

conditions) should represent an (unknown weighting) average over the nebula. It is interesting to compare IRAS18197–1118 with Abell 30 and Abell 58, although most probably the formation of IRAS18197–1118 has nothing to do with the born-again phenomenon of Abell 30 and Abell 58. These two PNe present old and much younger nebular ejections that contain completely different chemical abundances from each other (Guerrero & Manchado 1996). One might wonder about what chemical abundances would be obtained in Abell 30 and Abell 58 if they were spatially unresolved, and whether a comparison of these abundances with evolutionary models would indeed provide coherent and realistic information about their progenitor. It should be emphasized that evolutionary models, as those mentioned above, do not incorporate multiple, episodic ejections in the formation of PNe, as it is observed in many of these objects. Therefore, a proper comparison of observed and model abundances seems to require previous information about the morphology of the object. This may be particularly relevant for compact PNe and crucial for those presenting “peculiarities” in their chemical abundances, as IRAS18197–1118.

The Galactic coordinates and the estimated (statistical) distance of 6 kpc place IRAS18197–1118 in the inner Galactic disc. In fact, the radial velocity of the object ($V_{\text{LSR}} \simeq +95 \text{ km s}^{-1}$) fits very well in the distribution of radial velocity vs. Galactic longitude observed in inner-disc PNe (see Chiappini et al. 2009). Moreover, the radio continuum flux at 5 GHz of IRAS 18197–1118 ($\simeq 61 \text{ mJy}$, Urquhart et al. 2009) is lower than 100 mJy, and the size of the object (< 2.7 arcsec, see above) is much smaller than 10 arcsec, two criteria to be fulfilled by PNe located in the inner Galaxy (Stasińska et al. 1991; Chiappini et al. 2009). We also note that the high extinction towards the object points to a relatively large distance. Values of $c_{\text{H}\beta}$ comparable to or (much) higher than that observed in IRAS 18197–1118 are found in a number of inner-disc and bulge PNe, at distances > 5 kpc (e.g., Van de Steene & Jacoby 2001; Exter, Barlow & Walton 2004), whereas PNe at distances $\lesssim 4$ kpc usually present $c_{\text{H}\beta} \lesssim 2$ (see, e.g., Cappellaro et al. 2001; Giammanco et al. 2010). As for the abundances and abundance ratios, the values found in IRAS 18197–1118 are within the ranges observed in PNe in the inner Galactic regions (e.g., Henry et al. 2004; Exter et al. 2004; Cavichia et al. 2010).

A critical parameter in the analysis carried out above is the distance to IRAS 18197–1118. Through this paper we

have considered 6 kpc, which has been estimated from the statistical distance scale by Zhang (1995). Similar values for the distance of $\simeq 7$ kpc and $\simeq 6.3$ kpc are found with the distance scales by Van de Steene & Zijlstra (1995) and Bensby & Lundström (2001), respectively, providing support for the distance used in this paper. Nevertheless, some results suggest that statistical distances may not be suitable to analyze individual PNe (Tafuya et al. 2011; Miranda et al. 2012). Therefore, we consider it interesting to check whether the main conclusions of this investigation might critically depend on the distance value. To do this, we have considered a small and a large distance, namely, 2 and 10 kpc (i.e., 6 ± 4 kpc), to obtain the physical conditions and elemental abundances in IRAS 18197–1118, which should be compared with those obtained for 6 kpc. Table 4 lists the electron density, electron temperature, ionized mass, and elemental abundances for 2 and 10 kpc, derived using the same procedures as done for 6 kpc. In the 2–10 kpc distance range, the electron density and ionized mass are relatively high and low, respectively, and compatible with a relatively young PN. The helium abundance does not show a strong dependence on the distance and indicates a type I PN. The N/O abundance ratio is comparable to or smaller than that obtained for 6 kpc, and, in any case, lower than the value of 0.65–0.8, suggesting a type II PN (see above). Similarly, the nitrogen abundance remains much lower than typically observed in type I PNe, also suggesting a type II classification. A comparison of observed and model abundances, as done for 6 kpc (§ 3.4), also shows that the observed He abundance requires a more massive progenitor than indicated by the observed N and O abundances.

At a distance of about 10 kpc, IRAS 18197–1118 would still be located in the inner-disc. For distances of, say, $\lesssim 4$ kpc, IRAS 18197–1118 would be outside of the inner Galactic regions. However, the criteria of the radio continuum flux at 5 GHz and angular size of the object (see above) exclude ~ 90 –95% of PNe that are observed towards the inner Galaxy but do not belong to it (see Stasińska et al. 1991). Therefore, the probability that IRAS 18197–1118 is located at $\lesssim 4$ kpc is small. Moreover, as already mentioned, PNe at $\lesssim 4$ kpc, present values of $c_{\text{H}\beta}$ smaller than that found in IRAS 18197–1118. These comments argue in favor of IRAS 18197–1118 being located in the inner-disc and suggest that 6 kpc may be an approximate lower limit to the distance to the object.

5 CONCLUSIONS

We have presented an analysis of optical intermediate- and high-resolution spectra, 8.64 GHz radio continuum data, and narrow-band optical images of IRAS 18197–1118, a PN candidate whose nature, spectral properties and morphology had not been investigated before in detail. Our conclusions can be summarized as follows:

- The spectra confirm the PN nature of IRAS 18197–1118. A particularly high extinction ($c_{\text{H}\beta} \simeq 3.25$ –3.55) is obtained towards the object.
- The image at 8.64 GHz reveals a small (size $\simeq 2.7 \times 1.6$ arcsec²), point-symmetric elliptical PN, a bright compact central region, and possible bipolar jet-like features, indi-

cating several ejection events. The presence of a compact central nebula is unusual among PNe.

- An expansion velocity of $\simeq 20 \text{ km s}^{-1}$, a systemic velocity (LSR) of $\simeq +95 \text{ km s}^{-1}$, and a kinematical age of $\simeq 100 \times D[\text{kpc}] \text{ yr}$ are obtained for the object. The kinematical age suggests a relatively young PN.

- A relatively high electron density ($\simeq 3.4 \times 10^4 \text{ cm}^{-3}$) and a relatively small ionized mass ($\simeq 2.1 \times 10^{-2} M_{\odot}$) are derived from the 8.64 GHz radio continuum data for a distance of 6 kpc estimated from a statistical distance scale. Electron density and ionized mass also suggest a relatively young PN.

- A high He abundance is obtained but N is not enriched. The observed abundances cannot be reproduced in a consistent manner with standard evolutionary models, suggesting that the central region and the elliptical shell present different abundances. .

- The Galactic coordinates, radio continuum flux at 5 GHz, small angular size, systemic velocity and estimated distance of 6 kpc are consistent with IRAS 18197–1118 being an inner-disc PNe. The high extinction towards the object is also compatible with a relatively large distance.

- The main conclusions of this work do not critically depend on the distance to IRAS 18197–1118. Nevertheless, the properties of the object argue in favor of a distance $\gtrsim 6 \text{ kpc}$.

ACKNOWLEDGMENTS

We are very grateful to our referee, A. Zijlstra, for valuable comments that have improved the presentation and interpretation of the data. We thank Calar Alto Observatory for allocation of director's discretionary time to this programme. We are very grateful to the staff on Calar Alto for carrying out the observations. Discussions with A. García-Hernández and M.A. Guerrero are warmly acknowledged. We thank the staff of OAN-SPM, in particular to Mr. Gustavo Melgoza-Kennedy, for assistance during observations. LFM acknowledges partial support from Spanish MICINN AYA2011-30228-C3-01 grant (co-funded by FEDER funds). RV acknowledges support from grant UNAM-DGAPA-PAPIIT IN107914.

The investigation of IRAS 18197–1118 was suggested by Yolanda Gómez some years ago, when she found and analyzed the object in the VLA archive. We would like to dedicate this paper to the memory of Yolanda who passed away on 2012 February 16.

REFERENCES

- Bensby T., Lundström I., 2001, *A&A*, 374, 599
 Brocklehurst M., 1971, *MNRAS*, 153, 471
 Cappellaro E., Sabbadin F., Benetti S., Turatto M., 2001, *A&A*, 377, 1035
 Cavichia O., Costa R.D.D., Maciel W.J., 2010, *Rev.Mex. A&A*, 46, 159
 Chiappini C., Górný S.K., Stasińska G., Barbuy B., 2009, *A&A*, 494, 591
 Clegg R.E.S., 1987, *MNRAS*, 229, 31
 Condon J.J., Kaplan D.L., Terzian Y., 1999, *ApJS*, 123, 219
 Corradi R.L.M., Schwarz H.E., 1995, *A&A*, 293, 871
 Exter K.M., Barlow M.J., Walton N.A., 2004, *MNRAS*, 349, 1291
 Frew D.J., Parker Q.A., 2010, *PASA*, 27, 129
 Giammanco, C., et al., 2011, *A&A*, 525, A58
 Gómez L., Rodríguez L.F., Loinard L., 2013, *RMA&A*, 49, 79
 Gesicki K., Zijlstra A.A., Szyszka C., Hajduk M., Lagadec E., Guzmán-Ramírez L., 2010, *A&A*, 514, A54
 Guerrero M.A., Manchado A., 1996, *ApJ*, 472, 711
 Guerrero M.A., Miranda L.F., Manchado A., Vázquez R., 2000, *MNRAS*, 313, 1
 Helfand, D.J., Zoonematkermani S., Becker R.H., White R.L., 1992 *ApJS*, 80, 211
 Henry R.B.C., Kwitter K.B., Balick B., 2004, *AJ*, 127, 2284
 Howard J.W., Henry R.B.C., McCartney S., 1997, *MNRAS*, 284, 465
 Jacoby G.H., et al., 2010, *PASA*, 27, 156
 Karakas A.I., 2010, *MNRAS*, 403, 1413
 Kingsburgh R.L., Barlow M.J., 1994, *MNRAS*, 271, 257
 Kistiakowsky V, Helfand D.J., 1995, *AJ*, 110, 2225 (KH95)
 Maciel W.J., Köppen J., 1994, *A&A*, 282, 436
 Marigo P., 2001, *A&A*, 370, 194
 Meaburn J., López J.A., Gutiérrez L., Quiróz F., Murillo J.M., Valdéz J., Pedrayez, M., 2003, *Rev. Mex. A&A*, 39, 185
 Mezger P.G., Henderson A.P., 1967, *ApJ*, 147, 471
 Miranda L.F., Blanco M., Guerrero M.A., Riera A., 2012, *MNRAS*, 421, 1661
 Miranda L.F., Torrelles J.M., 1998, *ApJ*, 496, 274
 Miranda L.F., Vázquez R., Torrelles J.M., Eiroa C., López J.A., 1997, *MNRAS*, 288, 777
 Miszalski B., Parker Q.A., Acker A., Birkby J.L., Frew D.J., Kovacevic A., 2008, *MNRAS*, 384, 525
 Parker Q.A. et al., 2006, *MNRAS*, 373, 79
 Pottasch S.R., 1984, *Planetary nebulae (Reidel: Dordrecht)*
 Peimbert M., 1990, *Reports on Progress in Physics*, 53, 1559
 Pereira C.B., Miranda L.F., 2007, *A&A*, 467, 1249
 Ramos-Larios G., Guerrero M.A., Suárez O., Miranda L.F., Gómez J.F., 2012, *A&A*, 545, A20
 Seaton M.J., 1979, *MNRAS*, 187, 73
 Stasińska G., Tylenda R., Acker A., Stenholm B., 1991, *A&A*, 247, 173
 Stasińska G., Tylenda R., Acker A., Stenholm B., 1992, *A&A*, 266, 486
 Tafuya D. et al., 2011, *PASJ*, 63, 71
 Urquhart J.S. et al., 2009, *A&A*, 501, 539
 Van de Steene G.C., Jacoby G.H., 2001, *A&A*, 373, 536
 Van de Steene G.C., Zijlstra A.A., 1995, *A&A*, 293, 541
 Vázquez R., Kingsburgh R.L., López J.A., 1998, *MNRAS*, 296, 564
 Viironen K., et al., 2009, *A&A*, 504, 291
 Zhang C.Y., 1995, *ApJS*, 98, 659
 Zoonematkermani S., Helfand D.J., Becker R.H., White R.L., Perley R.A., 1990, *ApJS*, 74, 181